Observation of a Source and Seed Electron Three-belt Event in the Earth's Radiation Belts Based on Arase Satellite

Jia-Li Chen[1], Hong Zou[1], Yi-Xin Hao[2], Yu-Guang Ye[1], Yoshizumi Miyoshi[3], and Shi-ge Xu[1]

1 Institute of Space Physics and Applied Technology, Peking University, Beijing, China.

2 GFZ German Research Centre for Geosciences, Helmholtz Centre Potsdam, Potsdam, Germany.

3 Institute for Space-Earth Environmental Research, Nagoya University, Nagoya 464-8601, Japan.

Corresponding author: Hong Zou (hongzou@pku.edu.cn)

Key Points:

- We reported a source and seed electron three-belt event that occurred in October 2020 based on Arase observation.
- Electrons injected after the loss of the upper outer belt formed a new outer belt, possibly causing the three-belt structure to form.
- The fresh, substantial injected population during geomagnetic disturbances may disrupt the source and seed electron three-belt structure.

Abstract

The relativistic (~500 keV–2 MeV) and ultra-relativistic (~> 2 MeV) electron three-belt structure can originate from the partial depletion of the preexisting outer belt and replenishment of the new belt without direct electron injections. These processes may be related to radial diffusion caused by ULF (Ultra-Low Frequency) waves and local acceleration by VLF (Very-Low Frequency) waves. In this study, we reported a three-belt event with several hundred keV electrons based on Arase observation. The partial depletion of the outer belt and subsequent formation of a new belt due to source and seed electron (~30–500 keV) injection may be the primary mechanisms responsible for the three-belt structure. This discovery showed that the three-belt structure might not be limited to relativistic and ultra-relativistic electrons. Our study provided evidence for the existence of the source and seed electron three-belt structure, which could help improve our understanding of the radiation belt configuration.

Plain Language Summary

The electron radiation belts are regions of electrons surrounding Earth and usually exhibit a two-belt structure, i.e., the inner belt and the outer belt. The Van Allen Probes mission contributes to discovering ~> 600 keV electron three-belt structure in these regions, i.e., the lowest inner belt, the higher remnant belt, and the highest external outer belt. ULF (Ultra-Low Frequency) and VLF (Very-Low Frequency) waves are believed to contribute to the formation of this structure. However, substorm injections are not usually responsible for forming the external outer belt. In this study, based on Arase observation, we reported a three-belt event with mechanisms different from the above three-belt structure. In this event, electrons with several hundred keV energies exhibited a three-belt structure. We concluded that the partial depletion of the upper part of the original outer belt and the formation of the new outer belt due to substorm-injected source (~30–

200 keV) and seed (~200–500 keV) electrons might contribute to forming the structure. The discovery of the source and seed electron three-belt structure and the preliminary explanation of its cause in this study might help to improve our understanding of the structure and dynamics of the radiation belts.

1 Introduction

Ultra-relativistic electron three-belt structure is one of the significant discoveries of the Van Allen Probes mission. In September 2012, observations from the probes revealed the presence of a 'storage ring' between the inner and outer belts of ultra-relativistic electrons (~> 2 MeV) that lasted for about four weeks (Baker et al., 2013), resulting in a three-belt structure in the radiation belts including the inner belt, the remnant belt, and a new outer belt, also known as the external outer belt (Hao et al., 2020).

Based on the SAMPEX (Solar Anomalous, and Magnetospheric Particle Explorer) data sets from 1994 to 2003 that collected 110 CME-driven (CME, Coronal Mass Ejection) and 223 CIR-driven (CIR, Corotating Interaction Region) magnetic storms (Yue & Zong, 2011), Yuan and Zong (2013) identified 3 three-belt events from the CME-driven storms and 5 from the CIR-driven storms for 1.5–6.0 MeV electrons, which complemented the observational evidence of the three-belt events.

Observations of the three-belt structure mentioned above have generated significant research interest among scholars. In the following years, three related issues have been primarily discussed, namely, mechanisms for the partial depletion of the preexisting outer belt (i.e., the remnant belt), the formation of the new outer belt (i.e., the third belt or the external outer belt), and the decay of the remnant belt.

The solar wind dynamic pressure compresses the Earth's magnetosphere, leading to the magnetopause shadowing effect (e.g., Matsumura et al., 2011) followed by the excitation of ULF (Ultra-Low Frequency) waves and VLF (Very-Low Frequency) waves which may cause acceleration or loss of electrons by radial diffusion and local wave-particle interactions, respectively. The combined effect of magnetopause shadowing, ULF, and VLF waves may explain the formation of the remnant belt and the replenishment of the new outer belt (Loto'aniu et al., 2010; Mann et al., 2018; Mann et al., 2016; Yuri Y. Shprits et al., 2018; Yuri Y. Shprits et al., 2013; D. L. Turner et al., 2013; Drew L. Turner et al., 2012).

Victor A. Pinto et al. (2018) conducted a statistical study of 30 three-belt events occurring at 1.8–7.6 MeV from 2013 to 2017 based on Van Allen Probes data. They found that the decay time of the remnant belt increased with increasing energy. Furthermore, they observed that after the formation of the three-belt structure, the plasmapause location was restored above the remnant belt, protecting it from losses caused by various fluctuations outside the plasmasphere, thus allowing it to last longer (Victor A. Pinto et al., 2018; Thorne et al., 2013). Additionally, the decay rate of the remnant belt was consistent with the theoretical prediction of hiss wave scattering, suggesting that the pitch angle scattering caused by hiss waves may be the primary mechanism for the decay of the remnant belt (V. A. Pinto et al., 2019; Thorne et al., 2013).

In addition to the ultra-relativistic electron three-belt structure, Hao et al. (2020) found that relativistic electrons could also form a similar structure. Subsequently, Y.-X. Li et al. (2021) supplemented the statistic results of three-belt events in the energy range of 735 keV–1.8 MeV based on Van Allen Probes data. They also compared the results with those obtained from ultra-relativistic electron events. They found that three-belt events at energies $\sim<$ 1 MeV correlated

87 well with the SYM-H and AE (Auroral Electrojet) indices, indicating a potential relationship
88 between substorm injection and the formation of the structure at these energies.

89 The March 1991 sudden storm commencement (SSC) induced electron injection event (Blake et
90 al., 1992; X. Li et al., 1993) and the event when the electrons were accelerated to ~2–6 MeV in
91 the slot region during the 2003 Halloween storm (Baker et al., 2004; Y. Y. Shprits et al., 2006)
92 changed the two-zone configuration of the radiation belts. The involvement of externally injected
93 electrons is required to form the unusual structure in the 1991 events, moreover, injected
94 electrons needed to reach a lower L shell (McIlwain L parameter) to fill the slot region partially
95 (Baker et al., 2013; Blake et al., 1992; X. Li et al., 1993; Yuri Y. Shprits et al., 2013). In contrast,
96 electrons were required to be accelerated in the slot region to form a new belt during the
97 Halloween storm event (Baker et al., 2004; Y. Y. Shprits et al., 2006). The radiation belts during
98 the two events mentioned above exhibited distinctly different structures from the three-belt
99 structures formed by the depletion of the upper part of the preexisting outer belt and the
100 replenishment of the new outer belt.

101 In this study, with the support of Arase (also known as the ERG, Exploration of energization and
102 Radiation in Geospace) observation, we show that the source (~30–200 keV) and seed (~200–
103 500 keV) electrons (Koskinen & Kilpua, 2022, p. 214) at ~100–500 keV could also exhibit the
104 three-belt configuration, in addition to the existence of the three-belt structures in the energy
105 range above 600 keV. This discovery provides observational evidence for a source and seed
106 electron three-belt structure. Our study also indicates that this type of three-belt structure differed
107 from the aforementioned relativistic and ultra-relativistic ones in that its main mechanism may
108 be the loss of the outer belt partially and the formation of the new outer belt by lower energy
109 substorm-injected electrons. Our work is a complementary observation of the electron three-belt

structure in radiation belts that would likely help to improve the understanding of the radiation belt structures.

2 Data and Instruments

This study uses solar wind parameters, geomagnetic indices, and electron flux data. Specifically, the solar wind parameters are the Interplanetary Magnet field (IMF) magnitude B_t and its GSM (Geocentric Solar Magnetospheric coordinate system)-z component B_z, solar wind dynamic pressure P_{dyn}, and solar wind velocity V_{sw}. The geomagnetic indices are SYM-H (symmetric H-component) and SME (Newell & Gjerloev, 2011a, 2011b). The electron flux data are obtained from HEP-L (High-Energy Electron Experiments) onboard the Arase satellite and MEPED (Medium Energy Proton and Electron Detector) aboard the NOAA-18 satellite.

HEP-L detects electrons across 16 energy channels (70 keV–1 MeV), 15 pitch angle channels, and 16 azimuthal angle channels (Mitani et al., 2018b; Miyoshi et al., 2018b). We utilize its level-2 omnidirectional flux data (version v03_01, Mitani et al., 2018a) and level-3 orbit data (version v02, Miyoshi & Jun, 2018). Thanks to its orbit, HEP-L covers $L < 7$ and can detect most radiation belts in situ with a temporal resolution of 8 s (Mitani et al., 2018b), where L is the McIlwain's L parameter (McIlwain, 1961) for 90° pitch angles derived from the International Geomagnetic Reference Field model (Alken et al., 2021) and the Olson-Pfitzer Quiet model (Olson & Pfitzer, 1977). MEPED is mounted on the LEO (Low Earth Orbit) satellite, which orbits at an altitude of ~850 km. The instrument provides integrated flux at four energy channels above ~40 keV from the 0° and 90° telescope (Evans & Greer, 2004). The 0° telescope orients along the local zenith. Hence, it almost measures precipitating electrons at high latitudes. While the 90° telescope is mounted orthogonally to the 0° detector and is anti-parallel to the satellite

132 velocity vector, measuring trapped electrons at high latitudes (Babu et al., 2022; Evans & Greer,
133 2004; Kim et al., 2016) This study uses its version v01 data with 2 s resolution.

134 Data processing is applied to facilitate the analysis in this study. For the HEP-L data, a 180-data
135 window (corresponding to 24 min) of the Hampel filter (e.g., Davies & Gather, 2012; Pearson et
136 al., 2016) is used for outlier removal (outliers are deleted directly) followed by a 45-data window
137 (corresponding to 6 min) of sliding average for data smoothing. While for the NOAA-18 data,
138 only a sliding average of 120-data window (corresponding to 4 min) is applied. Notice that only
139 the processed flux data are used in this work.

3 Results

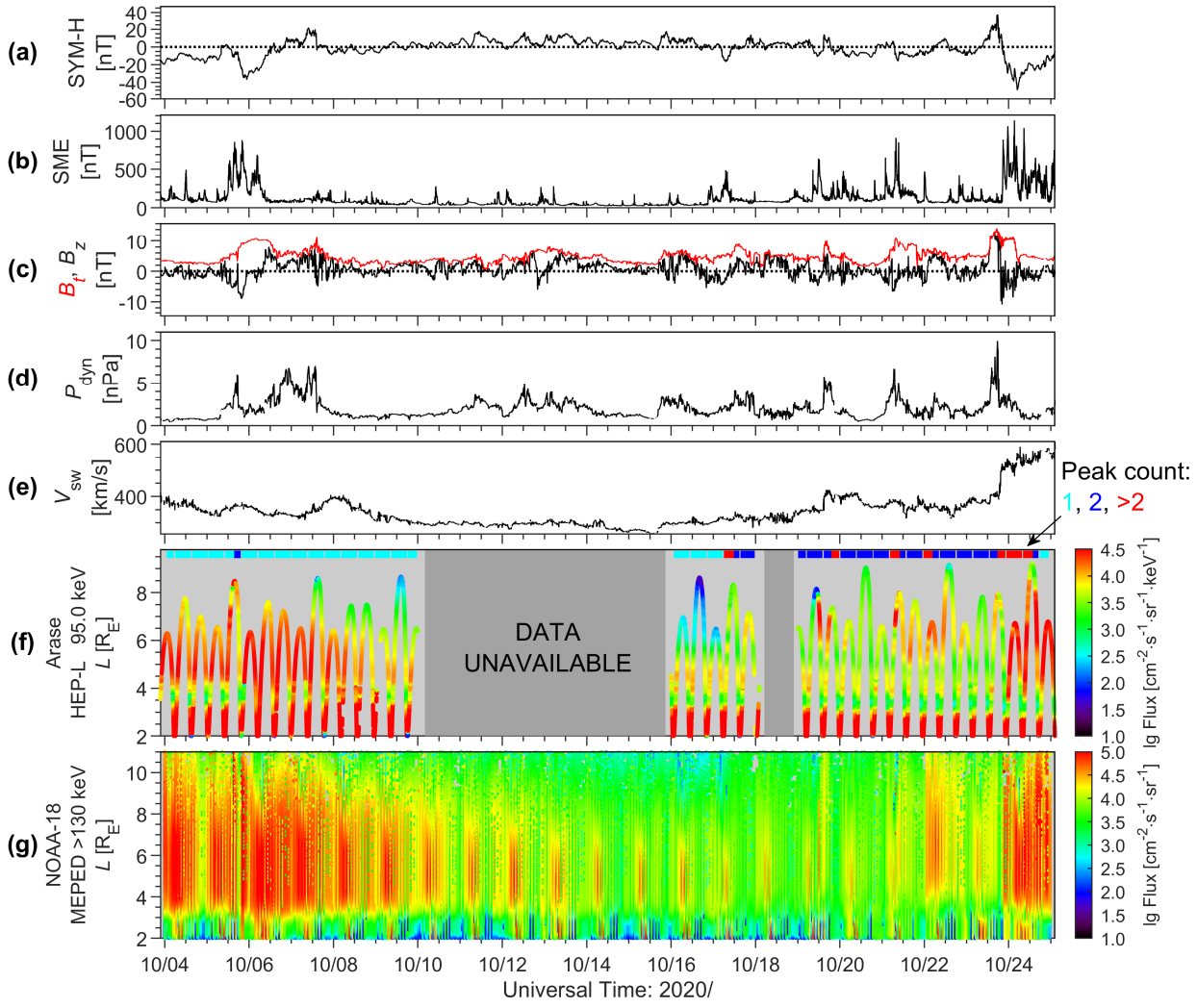
(a)
SYM-H [nT]
(b)
SME [nT]
(c)
B_t, B_z [nT]
(d)
P_{dyn} [nPa]
(e)
V_{sw} [km/s]
Peak count:
1, 2, >2
(f)
Arase HEP-L 95.0 keV
L [R_E]
DATA
UNAVAILABLE
lg Flux [cm^-2·s^-1·sr^-1·keV^-1]
(g)
NOAA-18 MEPED >130 keV
L [R_E]
lg Flux [cm^-2·s^-1·sr^-1]
10/04
10/06
10/08
10/10
10/12
10/14
10/16
10/18
10/20
10/22
10/24
Universal Time: 2020/

Figure 1. Solar wind parameters, geomagnetic indices, electron fluxes in the Arase HEP-L 95.0 keV energy channel and NOAA-18 MEPED 90° detector >130 keV energy channel during the source and seed electron three-belt event in the radiation belts in October 2020. (a)–(e) SYM-H, SME, B_t and B_z, P_{dyn}, and V_{sw}. (f) The electron differential flux with a central energy of 95.0 keV measured by the Arase HEP-L detector. The blue rectangles at the top indicate periods when two peaks are present in L profiles of the outer belt and others (cyan for one peak and red for three or more peaks) referring to Y.-X. Li et al. (2021). (g) >130 keV electron integrated flux measured by the NOAA-18 MEPED 90° detector.

3.1 Solar Wind and Geomagnetic Conditions for the Event

Figure 1 shows the geomagnetic indices (SYM-H, SME) and solar wind (B_t, B_z, P_{dyn}, V_{sw}) parameters from 4 to 25 October 2020, with 95.0 keV electron differential flux detected by the HEP-L detector and >130 keV electron integrated flux measured by the MEPED 90° detector. In Figure 1f, the blue rectangles depict instances where the L profiles of fluxes detected by Arase in the outer belt demonstrate two peaks, following the three-belt event criterion from Y.-X. Li et al. (2021). If the profiles don't meet this criterion, they are marked as having one peak or more than two peaks using cyan and red rectangles, respectively, based on the number of peaks with fluxes surpassing one-tenth of the maximum peak fluxes. Furthermore, if only two such peaks exist and their L-shell differs by less than 0.5, they are combined into one peak.

Figure 1a shows that from 5 to 6 October, the SYM-H index underwent a two-step decrease, reaching a minimum value of ~ -40 nT; B_t increased slowly with a dip at about 18:00 UT on 5 October; B_z exhibited a gradual increase followed by a brief decrease, then a final increase before falling to ~0. Meanwhile, V_{sw} increased and decreased slowly. These variations indicate an occurrence of a small storm. During the storm, several substorm injections indicated by SME occurred, and the injected electrons reached the inner magnetosphere, causing a transient double-peak distribution in the outer belt (as shown with blue rectangles at the top of Figure 1f). Following the storm, there was a continuous increase in 95.0 keV electron flux in the outer belt of $L > 4$ for ~1.5 days. The dynamic pressure (Figure 1d) enhanced the magnetopause current

and made the SYM-H increase to ~20 nT around 12:00 UT on 7 October. Then the SYM-H rapidly decreased to 0 and maintained small (~< 10 nT) fluctuations. Although the positive B_z did not trigger any obvious storms or substorms, 95.0 keV electron flux seemed to decrease subsequently.

The lack of valid Arase observation from 10 to 15 and 18 October is complemented by the NOAA-18 90° detector >130 keV electron flux data in Figure 1g. The low flux region varying with time appearing at L = 4–8 in panel (g) could be due to the pitch angle acquired by the detector and asymmetry in the latitudinal and longitudinal distribution of the radiation belt electrons in LEO (Zou et al., 2006). NOAA-18 observation indicates that the outer belt >130.0 keV electrons seemed to experience a slow decay during this period. The region with fluxes more than 10^5 $cm^{-2}s^{-1}sr^{-1}$ changed from L ~ 3.5–9.0 at 12:00 UT on 8 October to L = 3.5–6.5 at 00:00 UT on October 18. The contraction of the outer belt made it possible for electrons appearing near L = 6 to exist in isolation without combining with the preexisting outer belt, which is a precondition for the formation of the three-belt event.

3.2 Identification and Destruction of the Event

As Figure 1b shows, the SME increased to ~500 nT at about 06:00 UT on 17 October, indicating the occurrence of substorms (with more signatures discussed in Section 3.3). This was followed by a sudden enhancement of the electron flux in L~ 6–8, indicating a possible injection of source and seed electrons. However, the duration of this structure is uncertain due to the absence of Arase data on 18 October. At about 12:00 UT on 19 October, multiple substorms occurred with a sudden 1.5-day enhancement of the 95.0 keV electron flux near L = 7 to form a persistent structure. This structure separated from the original outer belt in L space and formed a new belt after 00:00 UT on 20 October. This belt, together with the original outer radiation belt (i.e., the

192 remnant belt), the low flux region between the two belts (the second 'slot region'), the inner belt,
193 and the slot region, formed the so-called three-belt structure, which we confirmed using the
194 criterion established by Y.-X. Li et al. (2021). The enhanced SME and 95.0 keV electron flux at
195 about 00:00 UT on 22 October indicated a substorm injection event, about which we show more
196 details in the next section. This also led to the formation of a three-belt structure lasting for ~ 36
197 hours.

198 Unless a new injected population arrived, the injected electrons were not bound around $L = 6$ for
199 long (~> 1.5 days). As shown in Figure 1f, the electron flux injected at 0:00 UT on 22 October
200 decreased after injection, reaching a low level at 12:00 UT on 23 October near $L = 6$. The
201 subsequent increase in electron flux during the next 6 hours may be due to the new injection and
202 will not be discussed in detail here. At around 12:00 UT on 23 October, a sudden increase in B_t,
203 P_{dyn}, and V_{sw} indicated the arrival of a shock near the Earth, which resulted in a magnetic storm
204 of about -50 nT at the smallest SYM-H, followed by several substorms. The electron flux at L ~
205 6 soon reached ~$10^{4.5}$ $cm^{-2}s^{-1}sr^{-1}keV^{-1}$, and the 'second slot' was filled so that the electron
206 radiation belts no longer exhibited a three-belt structure.
207

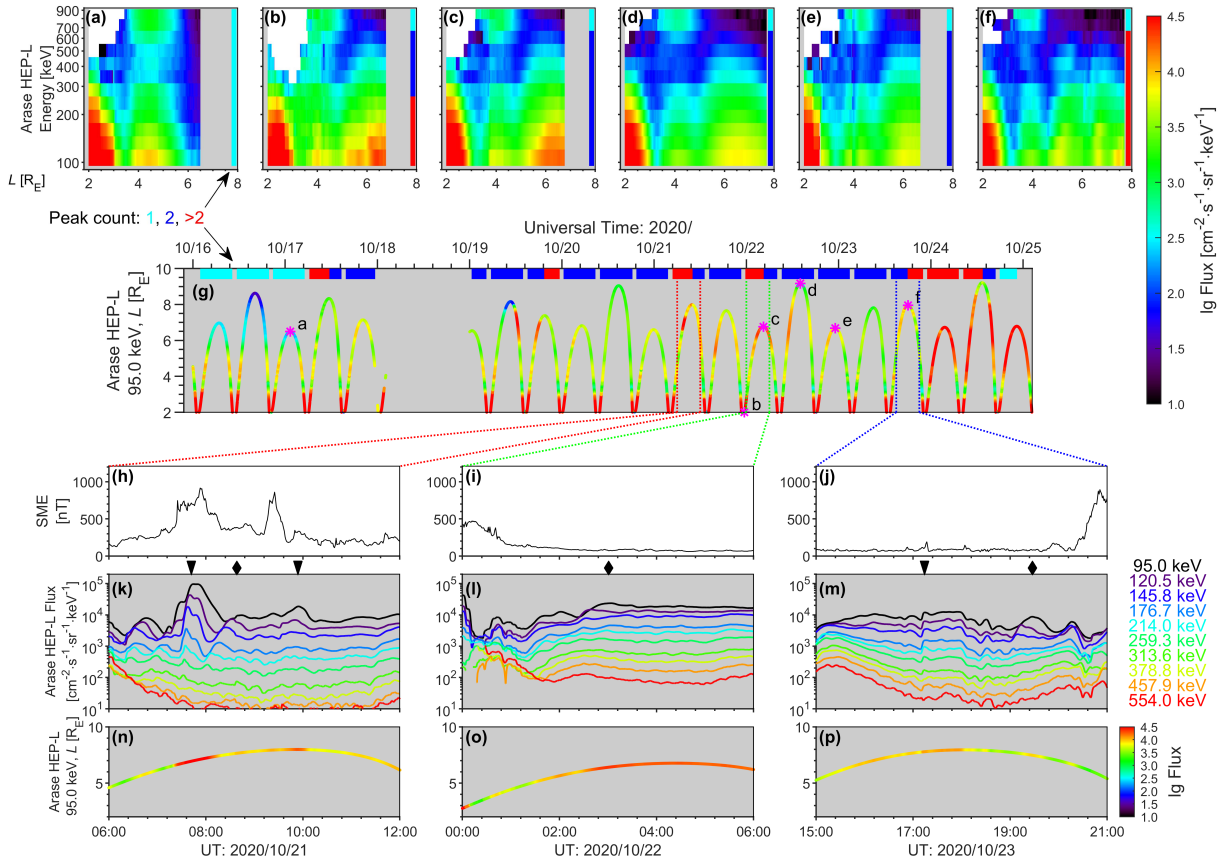

Figure 2. Energy spectra of the radiation belt electrons with three series of zoom-in views of SME index, electron fluxes versus time, as well as electron fluxes versus time and *L* shell from 16 to 25 October 2020. (a)–(f) electron energy spectra of Arase observation during different periods; (g) zoom-in view of 95.0 keV electron flux from Arase observation, the '*' and 'a'–'f' mark the start of the *L* profiles corresponding to panel (a)–(f). The rectangles at the top serve the same purpose as in Figure 1f. (h)–(j) zoom-in views of SME index during three periods; (k)–(m) zoom-in views of electron fluxes versus time, triangles above the three panels mark the moments when 95.0 keV electron injections were observed, while diamonds mark the moments when drift echoes were observed; (n)–(p) zoom-in views of electron fluxes versus time and *L* shell.

3.3 Observational Evidence of Main Substorm Injections and Energy Dependence of the Source Electron Three-belt Event

In this section, we investigate the energy dependence of the three-belt structure and provide more observational evidence of several obvious substorm injections. Figure 2 shows the energy spectra of the radiation belt electrons with zoom-in views from 16 to 25 October 2020. The rectangles at the top of Figure 2g perform the same function as in Figure 1f, and the '*' in this panel indicates

the start of the L profiles we have selected. White areas in panels (a)–(f) represent invalid data due to invalid counts and removed outliers, while gray areas indicate the background. Figures 2h–2p show signatures of several injections with triangles above Figures 2k–2m marking the moments when 95.0 keV electron injections were observed, while diamonds marking the moments when drift echoes were observed. In Figure 2a, the 100–300 keV electrons show a clear double-peak structure, i.e., an inner belt with $L < 3$ and an outer belt with $L \sim> 3.5$. The flux data of electrons with energy above 900 keV is not shown here. Besides, due to the limitation of the data quality and the variation of the inner belt with energy, it is not easy to distinguish the inner belt of electrons above 500 keV. However, since this paper focuses on the preexisting outer belt and the new outer belt of source and seed electrons, these limitations do not affect the conclusions.

Between about 05:00 UT on 17 and 00:00 UT on 22 October (after the corresponding moment of Figure 2a and before that of Figure 2b), three typical electron injection events occurred (at about 05:00 UT on 17, 12:00 UT on 19, and 07:00 UT on 21 October, respectively, ignoring 18 October due to missing data). Figures 2h, 2k and 2n show more details about the third injection, in which energy dispersion and drift echo signatures could be observed. These injections resulted in double-peak or even multi-peak (three peaks or more) structures in the outer belt. The multi-peak structures appeared soon after the substorm-injected electrons reached the inner magnetosphere, probably drift echoes of the injected electrons or a new less obvious injection as is shown in Figure 2k. The double-peak structure persisted for about 24 hours after the second injection, meeting the criterion for a three-belt event established by Y.-X. Li et al. (2021). To analyze the response of electrons with different energies during the event more coherently, we

246 focus more on the event starting at ~00:00 UT on 22 October with the three-belt structure lasting
247 for ~36 hours.

248 The SME index increased to ~500 nT at ~00:24 UT on 22 October, which may indicate a
249 substorm injection. However, there was no injection signature observed by Arase due to its
250 location at this moment. About 2.5 hours later, the 95.0 keV electrons increased, probably drift
251 echoes corresponding to the previous substorm injection as is shown in Figure 2l. This indirectly
252 proved the occurrence of the substorm injection at 00:24 UT. As Figure 2b shows, this injection
253 led to three or more peaks in the outer belt for L ~ 3–7 with energies less than ~250 keV and two
254 peaks in the outer belt for electrons with energies between 250 and 700 keV. While for the
255 higher energy, the flux did not increase significantly around L = 6, indicating that there are
256 relatively few electrons with this energy in the injected population. Therefore, the outer belt
257 failed to show a double-peak structure. Figure 2c–2e shows the preexisting outer belt near L ~ 4
258 and the new outer belt at L ~ 6.5 with an energy range of 100–700 keV during the event.

259 Around the start of the period shown in Figure 2f, the arrival of a shock triggered a magnetic
260 storm with a minimum SYM-H of ~-50 nT and several substorms with a maximum SME of
261 ~1000 nT (Figure 1a–1b), accompanied by onsets of injection events. As shown in Figure 2f, the
262 outer belt of electrons with energies of 100–700 keV showed more than three peaks, indicating
263 that electron injection accompanied by recurrent drift echoes occurred in these energy channels,
264 with more signatures shown in Figure 2j, 2m and 2p. Around 12:00 UT on 24 October, multiple
265 peaks in the outer radiation belt merged, and the radiation belts reverted to the typical double-
266 belt structure (Figure 2g and curve #8 in Figure 3a).

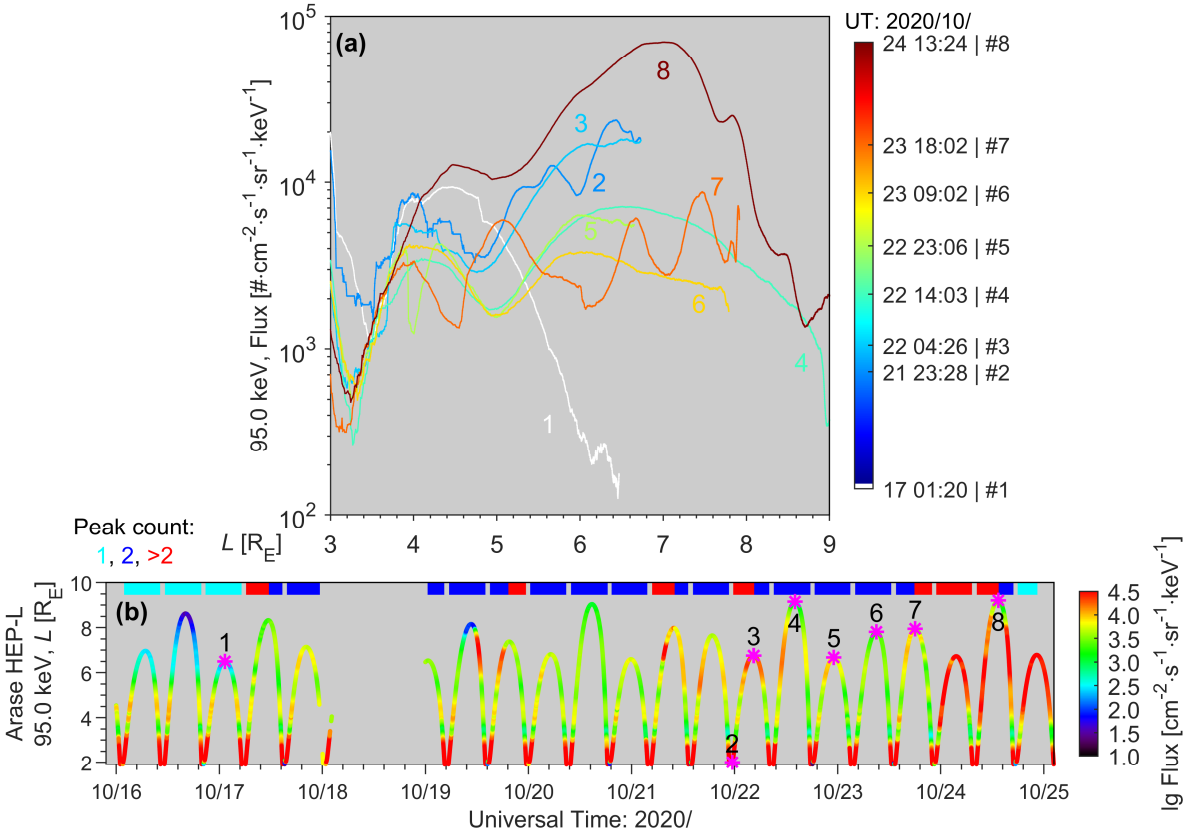

Figure 3. Evolution of the 95.0 keV electron flux from 16 to 25 October 2020. (a) Variation of 95.0 keV electron flux measured by Arase with time and *L*-value (in the form of a graph), colors of the different curves correspond to different periods; (b) Variation of 95.0 keV electron flux measured by Arase with time and *L*-value (in the form of a scatter plot), the function of the rectangles at the top is the same as in Figure 1f and Figure 2g.

3.4 Evolution of the Source and Seed Electron Three-belt Event

In this section, we present the 95.0 keV electron differential flux with time to show the evolution of this event in detail. As in Figure 1f and Figure 2g, the 95.0 keV electron flux and rectangles indicating the number of peaks in the outer belt are also shown in Figure 3b to give an overview of the event and to indicate the chosen profiles.

We show eight typical curves in Figure 3a. The first curve marked in white indicates the variation of the electron flux with the *L*-value before injections when the radiation belts did not exhibit a three-belt structure. Although there was a peak in the flux around $L = 6.2$ during this

time, we only consider this as a nominal one-peak structure in the outer belt because the corresponding electron flux is less than 0.1 of the peak flux (Y.-X. Li et al., 2021), and all similar configurations are not considered as a double-peak structure in the outer belt. For the absence of data and the ignoring of events with shorter duration, we focus on the longest sustained event that occurred at ~00:00 UT on 22 October. As shown in Figure 3a, curve #2 shows multiple peaks, which may originate from injection populations and the corresponding drift echoes (Figure 2l). Curve #3 shows that the multi-peak structure of the outer belt had merged. Due to the limitation of the satellite orbit, this curve only extended to $L \sim 7$. However, thanks to the presence of a clear peak at $L = 4$ and the disappearance of multi-peak structure around $L = 4$–7, we can still conclude that a double-peak structure appeared in the outer belt at that time, i.e., the three-belt structure began to emerge.

Curves #3–#6 curves exhibited double-peak structures (ignoring the dip in curve #5 due to failure count at $L \sim 4$) with a time difference of more than one day, confirming a valid 95.0 keV three-belt event occurred. The peak flux in the third belt decreased, while that in the remnant belt didn't decrease monotonically, except when checked over a longer period. Curve #7 again shows multiple peaks, which may also be due to a new injection as well as the corresponding drift echoes (Figures 2m and 2p), and also implies the disappearance of the three-belt structure. Curve #8, starting at 13:24 UT on 24 October, shows that the multi-peak structure merged with the remnant belt, and the radiation belts finally returned to the double-belt structure.

4 Discussion

Compared to relativistic and ultra-relativistic three-belt events that occurred without direct injection, the main distinguishing feature of the event in this study may lie in the energy in which

it occurred. The lower energy may determine the mechanism behind the formation of the new outer belt and the duration of the entire structure.

In the present observation, the new outer belt of the three-belt event may originate directly from injections rather than from the gradual replenishment so that this structure could form within a few hours after injections. In contrast, in three-belt events without corresponding energy electron injections (including relativistic and ultra-relativistic electrons), the new outer belts are replenished more slowly, which may originate from the inward radial diffusion caused by ULF waves and the local acceleration caused by VLF waves (Loto'aniu et al., 2010; Mann et al., 2018; Mann et al., 2016; Yuri Y. Shprits et al., 2018; Yuri Y. Shprits et al., 2013; D. L. Turner et al., 2013; Drew L. Turner et al., 2012). The substorm-injected source and seed electrons may be accelerated to become relativistic. Consequently, the new outer belts in relativistic and ultra-relativistic three-belt events may come from the acceleration of lower energy electrons from injections in some cases.

The duration of the structure in relativistic and ultra-relativistic three-belt events without direct injections may be determined by the duration of the remnant belt unless a strong perturbation destroys the structure. In such cases, the structure usually disappears only when the remnant belt vanishes. In addition, the hiss scattering influences the duration of the relativistic and ultra-relativistic electron remnant belts (V. A. Pinto et al., 2019; Thorne et al., 2013). For the source and seed electron three-belt event reported here, the decay of the new outer belt may be faster than that of the remnant belt due to scattering to the atmosphere or being accelerated to higher energies. Consequently, the duration of this structure may depend more on the duration of the new outer belt than that of the remnant belt. However, the ~100–500 keV electrons are also vulnerable to loss due to hiss wave scattering (Ma et al., 2016). The remnant belt in this study

lasts for more than a week, which is much longer than the duration of the belt in the ~600 keV three-belt event reported by Hao et al. (2020). The difference in remnant belt duration between the two events could be attributed to the intensity of the hiss and chorus waves as remnant belts may not always be inside the plasmasphere. However, this is not discussed in detail in this paper and could be a topic for future research.

5 Conclusions

In this study, we report a source and seed electron three-belt event in the radiation belts. Our conclusions are listed as follows:

1. Two source and seed electron three-belt events occurred with a maximum duration of 1.5 days after several substorms indicated by the SME and a sudden increase of 95.0 keV electrons from 19 to 24 October.

2. The electron three-belt structures are not strictly confined to relativistic (~> 500 keV) or ultra-relativistic (>2 MeV) energies. Source and seed electrons may also exhibit a similar structure.

3. Source and seed electron injection may induce the formation of a three-belt event preceded by partial loss of the preexisting outer belt.

4. The vanishment of the new outer belt or a new injection may disrupt the three-belt structure.

Acknowledgments

Arase (ERG) data were obtained from the ERG Science Center operated by ISAS/JAXA and ISEE/Nagoya University (Miyoshi et al., 2018a). We acknowledge the Arase (ERG) team,

NOAA-18 team, NASA's Space Physics Data Facility, and SuperMAG collaboration for providing data for this study. This work was supported by the National Natural Science Foundation of China 42274225.

Open Research

Arase (ERG) HEP-L v03_01 data (10.34515/DATA.ERG-01001) and Orbit L3 v02 data (10.34515/DATA.ERG-12001) were obtained from the ERG Science Center (https://ergsc.isee.nagoya-u.ac.jp/data_info/erg.shtml.en). NOAA-18 MEPED data were available from https://cdaweb.gsfc.nasa.gov/pub/data/noaa/noaa18/sem2_fluxes-2sec/2020/ provided by NASA's Space Physics Data Facility. Interplanetary magnetic field, solar wind dynamic pressure, and solar wind velocity were provided by NASA OMNI database (https://omniweb.gsfc.nasa.gov/). SME data were available from https://supermag.jhuapl.edu/mag/?fidelity=low&start=2001-01-29T16%3A00%3A00.000Z&interval=23%3A59 supported by SuperMAG collaboration.

References

Alken, P., Thébault, E., Beggan, C. D., Amit, H., Aubert, J., Baerenzung, J., et al. (2021). International Geomagnetic Reference Field: the thirteenth generation. *73*(1), 49. https://doi.org/10.1186/s40623-020-01288-x

Babu, E. M., Tyssøy, H. N., Smith - Johnsen, C., Maliniemi, V., Salice, J. A., Millan, R. M., & Richardson, I. G. (2022). Determining Latitudinal Extent of Energetic Electron Precipitation Using MEPED On - Board NOAA/POES. *127*(9). https://onlinelibrary.wiley.com/doi/10.1029/2022JA030489

Baker, D. N., Kanekal, S. G., Hoxie, V. C., Henderson, M. G., Li, X., Spence, H. E., et al. (2013). A Long-Lived Relativistic Electron Storage Ring Embedded in Earth's Outer Van Allen Belt. *340*(6129), 186-190. https://www.science.org/doi/abs/10.1126/science.1233518%J Science

Baker, D. N., Kanekal, S. G., Li, X., Monk, S. P., Goldstein, J., & Burch, J. L. (2004). An extreme distortion of the Van Allen belt arising from the 'Hallowe'en' solar storm in 2003. [2005 Macmillan Magazines Ltd.]. *432*(7019), 878-881. https://www.nature.com/articles/nature03116

Blake, J. B., Kolasinski, W. A., Fillius, R. W., & Mullen, E. G. (1992). Injection of electrons and protons with energies of tens of MeV into L < 3 on 24 March 1991. *19*(8), 821-824. https://onlinelibrary.wiley.com/doi/abs/10.1029/92GL00624

Davies, L., & Gather, U. (2012). The Identification of Multiple Outliers. [Copyright Taylor and Francis Group, LLC]. https://www.tandfonline.com/doi/abs/10.1080/01621459.1993.10476339

Evans, D., & Greer, M. (2004). *Polar orbiting environmental satellite space experiment monitor-2: Instrument descriptions and archive data documentation*. Retrieved from https://ngdc.noaa.gov/stp/satellite/poes/docs/SEM2Archive.pdf

Hao, Y. X., Zong, Q.-G., Zhou, X.-Z., Zou, H., Rankin, R., Sun, Y. X., et al. (2020). A Short-lived Three-Belt Structure for sub-MeV Electrons in the Van Allen Belts: Time Scale and Energy Dependence. *125*(9), e2020JA028031. https://onlinelibrary.wiley.com/doi/abs/10.1029/2020JA028031

Kim, K.-C., Shprits, Y. Y., & Blake, J. B. (2016). Fast injection of the relativistic electrons into the inner zone and the formation of the split-zone structure during the Bastille Day storm in July 2000. *121*(9), 8329-8342. https://onlinelibrary.wiley.com/doi/abs/10.1002/2015JA022072

Koskinen, H. E. J., & Kilpua, E. K. J. (2022). *Physics of Earth's Radiation Belts: Theory and Observations*. Cham: Springer International Publishing.

Li, X., Roth, I., Temerin, M., Wygant, J. R., Hudson, M. K., & Blake, J. B. (1993). Simulation of the prompt energization and transport of radiation belt particles during the March 24, 1991 SSC. *20*(22), 2423-2426. https://onlinelibrary.wiley.com/doi/abs/10.1029/93GL02701

Li, Y.-X., Yue, C., Hao, Y.-X., Zong, Q.-G., Zhou, X.-Z., Fu, S.-Y., et al. (2021). The Characteristics of Three-Belt Structure of Sub-MeV Electrons in the Radiation Belts. *126*(7), e2021JA029385. https://onlinelibrary.wiley.com/doi/abs/10.1029/2021JA029385

Loto'aniu, T. M., Singer, H. J., Waters, C. L., Angelopoulos, V., Mann, I. R., Elkington, S. R., & Bonnell, J. W. (2010). Relativistic electron loss due to ultralow frequency waves and enhanced outward radial diffusion. *115*(A12). https://onlinelibrary.wiley.com/doi/abs/10.1029/2010JA015755

Ma, Q., Li, W., Thorne, R. M., Bortnik, J., Reeves, G. D., Kletzing, C. A., et al. (2016). Characteristic energy range of electron scattering due to plasmaspheric hiss. *121*(12), 11,737-711,749. https://onlinelibrary.wiley.com/doi/abs/10.1002/2016JA023311

Mann, I. R., Ozeke, L. G., Morley, S. K., Murphy, K. R., Claudepierre, S. G., Turner, D. L., et al. (2018). Reply to 'The dynamics of Van Allen belts revisited'. [2018 Nature Publishing Group, a division of Macmillan Publishers Limited. All Rights Reserved.]. *14*(2), 103-104. https://www.nature.com/articles/nphys4351

Mann, I. R., Ozeke, L. G., Murphy, K. R., Claudepierre, S. G., Turner, D. L., Baker, D. N., et al. (2016). Explaining the dynamics of the ultra-relativistic third Van Allen radiation belt. [2016 Nature Publishing Group]. *12*(10), 978-983. https://www.nature.com/articles/nphys3799

Matsumura, C., Miyoshi, Y., Seki, K., Saito, S., Angelopoulos, V., & Koller, J. (2011). Outer radiation belt boundary location relative to the magnetopause: Implications for magnetopause shadowing. [Copyright 2011 by the American Geophysical Union.]. *116*(A6). https://onlinelibrary.wiley.com/doi/abs/10.1029/2011JA016575

McIlwain, C. E. (1961). Coordinates for mapping the distribution of magnetically trapped particles. *66*(11), 3681-3691. https://onlinelibrary.wiley.com/doi/abs/10.1029/JZ066i011p03681

Mitani, T., Hori, T., Park, I., Takashima, T., Miyoshi, Y., & Shinohara, I. (2018a). Exploration of energization and Radiation in Geospace (ERG) HEP Level-2 omni-directional flux data (Publication no. 10.34515/DATA.ERG-01001). from ERG Science Center, Institute for Space-Earth Environmental Research, Nagoya University https://doi.org/10.34515/DATA.ERG-01001

Mitani, T., Takashima, T., Kasahara, S., Miyake, W., & Hirahara, M. (2018b). High-energy electron experiments (HEP) aboard the ERG (Arase) satellite. *70*(1), 77. https://doi.org/10.1186/s40623-018-0853-1

Miyoshi, Y., Hori, T., Shoji, M., Teramoto, M., Chang, T. F., Segawa, T., et al. (2018a). The ERG Science Center. *70*(1), 96. https://doi.org/10.1186/s40623-018-0867-8

Miyoshi, Y., & Jun, C.-W. (2018). Exploration of energization and Radiation in Geospace (ERG) Orbit Level-3 data. In: ERG Science Center, Institute for Space-Earth Environmental Research, Nagoya University.

Miyoshi, Y., Shinohara, I., Takashima, T., Asamura, K., Higashio, N., Mitani, T., et al. (2018b). Geospace exploration project ERG. *70*(1), 101. https://doi.org/10.1186/s40623-018-0862-0

Newell, P. T., & Gjerloev, J. W. (2011a). Evaluation of SuperMAG auroral electrojet indices as indicators of substorms and auroral power. *116*(A12). https://onlinelibrary.wiley.com/doi/abs/10.1029/2011JA016779

Newell, P. T., & Gjerloev, J. W. (2011b). Substorm and magnetosphere characteristic scales inferred from the SuperMAG auroral electrojet indices. *116*(A12). https://onlinelibrary.wiley.com/doi/abs/10.1029/2011JA016936

Olson, W. P., & Pfitzer, K. A. (1977). *Magnetospheric magnetic field modeling. Annual scientific report*. Retrieved from https://www.osti.gov/biblio/7212748

Pearson, R. K., Neuvo, Y., Astola, J., & Gabbouj, M. (2016). Generalized Hampel Filters. *2016*(1), 87. https://doi.org/10.1186/s13634-016-0383-6

Pinto, V. A., Bortnik, J., Moya, P. S., Lyons, L. R., Sibeck, D. G., Kanekal, S. G., et al. (2018). Characteristics, Occurrence, and Decay Rates of Remnant Belts Associated With Three-Belt Events in the Earth's Radiation Belts. *45*(22), 12,099-012,107. https://onlinelibrary.wiley.com/doi/abs/10.1029/2018GL080274

Pinto, V. A., Mourenas, D., Bortnik, J., Zhang, X.-J., Artemyev, A. V., Moya, P. S., & Lyons, L. R. (2019). Decay of Ultrarelativistic Remnant Belt Electrons Through Scattering by Plasmaspheric Hiss. *124*(7), 5222-5233. https://onlinelibrary.wiley.com/doi/abs/10.1029/2019JA026509

Shprits, Y. Y., Horne, R. B., Kellerman, A. C., & Drozdov, A. Y. (2018). The dynamics of Van Allen belts revisited. [2018 Nature Publishing Group, a division of Macmillan Publishers Limited. All Rights Reserved.]. *14*(2), 102-103. https://www.nature.com/articles/nphys4350

Shprits, Y. Y., Subbotin, D., Drozdov, A., Usanova, M. E., Kellerman, A., Orlova, K., et al. (2013). Unusual stable trapping of the ultrarelativistic electrons in the Van Allen radiation belts. [2013 Nature Publishing Group]. *9*(11), 699-703. https://www.nature.com/articles/nphys2760

Shprits, Y. Y., Thorne, R. M., Horne, R. B., Glauert, S. A., Cartwright, M., Russell, C. T., et al. (2006). Acceleration mechanism responsible for the formation of the new radiation belt during the 2003 Halloween solar storm. *33*(5). https://onlinelibrary.wiley.com/doi/abs/10.1029/2005GL024256

Thorne, R. M., Li, W., Ni, B., Ma, Q., Bortnik, J., Baker, D. N., et al. (2013). Evolution and slow decay of an unusual narrow ring of relativistic electrons near L 3.2 following the September 2012 magnetic storm. *40*(14), 3507-3511. https://onlinelibrary.wiley.com/doi/abs/10.1002/grl.50627

Turner, D. L., Angelopoulos, V., Li, W., Hartinger, M. D., Usanova, M., Mann, I. R., et al. (2013). On the storm-time evolution of relativistic electron phase space density in Earth's outer radiation belt. *118*(5), 2196-2212. https://onlinelibrary.wiley.com/doi/abs/10.1002/jgra.50151

Turner, D. L., Shprits, Y., Hartinger, M., & Angelopoulos, V. (2012). Explaining sudden losses of outer radiation belt electrons during geomagnetic storms. [2012 Nature Publishing Group]. *8*(3), 208-212. https://www.nature.com/articles/nphys2185

Yuan, C., & Zong, Q. (2013). The double-belt outer radiation belt during CME- and CIR-driven geomagnetic storms. *118*(10), 6291-6301. https://onlinelibrary.wiley.com/doi/abs/10.1002/jgra.50564

Yue, C., & Zong, Q. (2011). Solar wind parameters and geomagnetic indices for four different interplanetary shock/ICME structures. *116*(A12). https://onlinelibrary.wiley.com/doi/abs/10.1029/2011JA017013

Zou, H., Xiao, Z., Hao, Y., Zou, J., Zhu, W., Wu, Z., & Xiang, H. (2006). Analysis of the observation of particle detector inside 'CBERS-1' satellite under solar quiet conditions. *49*(3), 342-357. https://doi.org/10.1007/s11431-006-0342-9